Research Square

Preprints are preliminary reports that have not undergone peer review.
They should not be considered conclusive, used to inform clinical practice,
or referenced by the media as validated information.

Box–Behnken–Optimized Essential-Oil–Alcohol Hand Rub Shows in-vitro Activity Against SARS-CoV-2, Dengue, Influenza A, Measles, Chikungunya, and Nipah

Ilyas Uoorakkottil

dr.ilyasmcp@gmail.com

Moulana College of Pharmacy

Rashid K

Moulana College of Pharmacy

Sivakumar Annadurai

King Khalid University

Mohammed Muqtader Ahmed

Prince Sattam Bin Abdulaziz University

Abdul vajid

Moulana College of Pharmacy

Artha Rajagopal

Moulana College of Pharmacy

Article

Keywords: Essential oils, eugenol, terpinen-4-ol, trans-anethole, Box–Behnken design, in-silico docking (Glide/MM-GBSA, OPLS4), EN 14476 virucidal assay, SARS-CoV-2, Dengue, Influenza A, Measles, Chikungunya, Nipah, virucidal activity

Posted Date: October 13th, 2025

DOI: https://doi.org/10.21203/rs.3.rs-7536424/v1

License: This work is licensed under a Creative Commons Attribution 4.0 International License.
Read Full License

Additional Declarations: No competing interests reported.

Abstract

Aim: To develop and optimize an alcohol-anchored, essential-oil–augmented hand rub (EO-ABHR) that improves early-contact virucidal performance without compromising regulatory alcohol content.
Methods: EO actives (eugenol, terpinen-4-ol, trans-anethole) were prioritized in silico via a standardized Schrödinger pipeline (LigPrep/Epik; Glide SP→XP; Prime MM-GBSA, OPLS4) against six crystallographically validated viral targets (6LU7, 3TRK, 7SKS, 1TG8, 2ZTT, 2VSM). A 3-factor, 3-level Box–Behnken design (17 runs; factors: EO ratio, glycerin, aloe) was applied to an isopropyl-alcohol base to balance MIC, viscosity, spreadability, pH, and evaporation; cytotoxicity (CC_{50}) constrained test ceilings.
Results: Docking/MM-GBSA ranked eugenol highest overall (notably at 2ZTT and 1TG8), followed by terpinen-4-ol, with anethole weakest (especially at 2VSM). Response-surface modeling showed an excellent quadratic fit for viscosity (R^2=0.9987; R^2_adj=0.9958) and an acceptable fit for MIC (R^2=0.7146). EO ratio primarily drove MIC, glycerin governed viscosity, and aloe improved spreadability with minimal viscosity penalty. The optimized ABHR met target CQAs (viscosity 1.47–5.09 cP; pH ~5–7; rapid evaporation) and achieved EO MICs of 739–1034 ng·mL^{-1}. In vitro, it produced contact-time–dependent reductions in infectivity across six matched virus–cell systems, modestly outperforming an alcohol-only control within CC_{50}-informed safety bounds.
Conclusion: An integrated docking→MM-GBSA→DoE workflow linked EO prioritization to an alcohol-compliant ABHR with broad in-vitro activity. Alcohol remained the dominant virucidal driver, while eugenol/terpinen-4-ol–enriched blends yielded adjunct gains in early-time performance and user-centric attributes, providing a reproducible route to performance-tuned EO-ABHRs.

Introduction

Handwashing remains a major intervention for interrupting respiratory and contact transmission of pathogens through community and healthcare environments. Alcohol-based hand rubs (ABHRs) are recommended by worldwide bodies due to fast onset of action, sheer antimicrobial spectrum, and ease of utilization at the place of care. The World Health Organization (WHO) and the U.S. Centers for Disease Control and Prevention (CDC) recommend ABHR composition containing ≥ 60% alcohol, giving standardized recipes that can be locally produced to assure uninterrupted supply in times of surge or disruptive supply chains [1, 2]. Though alcohol alone provides a dependable viricidal action, primarily through lipid envelope disruption and protein denaturation, there is a resurgence in research interest into plant-based essential oils (EOs) being used as adjuvants to complementarize the alcohol effect and to enhance user acceptance through agreeable scents and feels on the skin. Many EOs and their major components have shown in vitro activity against viruses/virucidal, bacteria, toxins, and inflammation, suggesting their logic for topical antiseptics [3–7]. Most recurrent lead components of these include eugenol (clove), terpinen-4-ol (tea tree oil), and trans-anethole (anise/star-anise): reports suggest that eugenol may inhibit influenza viruses and herpesviruses; tea tree oil, with high terpinen-4-ol content, inhibits influenza A in cell culture and aerosol models; and anethole extracts show activity against HSV in vitro [3–6, 8–9]. Taken together, these results support a systematic evaluation of China constituents as functional counterparts in ABHRs. Alongside wet-lab testing, molecular docking in silico can prioritize

candidate phyto-chemicals against relevant viral proteins by evaluating shape/chemical complementarity, interaction networks, and putative binding free energies prior to bench validation [10–14]. In this study, the six structurally validated proteins representing high-priority pathogens with high-quality crystallographic data available are SARS-CoV-2 main protease (6LU7) [15], chikungunya nsP2 protease (3TRK) [16], measles virus matrix protein (7SKS) [17], dengue virus E glycoprotein fragment (1TG8) [18], influenza A polymerase PB1–PB2 interface (2ZTT) [19], and Nipah virus attachment glycoprotein bound to ephrin-B2 (2VSM) [20]. We employ a Schrödinger workflow comprising Protein Preparation Wizard for structure standardization, SiteMap for binding-site identification/druggability, and Glide SP→XP for docking and pose discrimination, and Prime MM-GBSA (VSGB 2.0) for rescoring and per-residue energy decomposition [21]. Alongside this, the OPLS4 force field is applied for improved energetics and nonbonded interactions of small molecules, which are especially relevant to phenylpropanoids/terpenoids such as eugenol, terpinen-4-ol, and anethole. Computational rank-ordering and interaction maps produced from this study are further employed to assist formulation decisions for an ABHR comprising glycerol and aloe vera gel (for soothing and spreadability). Formulation science is also crucial for practical effectiveness of ABHRs, the latter of which depends on not only the actives but also the physicochemical and sensory attributes that are dose delivery, coverage, residence-time, and user adherence. These attributes, such as viscosity, spreadability/evaporation time, pH, and organoleptic profile, may affect perceived quality and antimicrobial contact effectiveness. To create a rational balance between these attributes and biologically-quantified antimicrobial performance, RSM is implemented-the Box–Behnken design (BBD) in particular provides a great way to explore curvature and interaction among a few factors with a minimum number of runs [22–25]. In our case, the three formulation parameters (EO ratio, glycerin, aloe) are co-optimized for MIC (an antimicrobial proxy) and viscosity, with the other sensory attributes maintained within an acceptable band. From a public-health perspective, maintaining ABHRs at or above WHO/CDC alcohol limits is a hard-and-fast rule, but carefully chosen EO constituents should confer complementary secondary mechanisms on top of that—membrane perturbation, hydrophobic enclosure within viral protein pockets, and local anti-inflammatory effects—while improving acceptability, which in turn improves compliance. Biologically, eugenol, terpinen-4-ol, and anethole stand out since they have each demonstrated in vitro antiviral trends against enveloped viruses and bear physicochemical characteristics (moderate lipophilicity, H-bonding capacity, aromatic systems) amenable to stable interaction within shallow, hydrophobic protein sites. A target-guided approach—docking and MM-GBSA against 6LU7, 3TRK, 7SKS, 1TG8, 2ZTT, and 2VSM—shall prioritize which of these small molecules is most likely to engage with each protein pocket via hydrogen bonds, π–π/cation–π interactions, hydrophobics, and salt bridges. Finally, the RSM/BBD framework is justified to channel computational leads into a statistically optimized ABHR where EO ratio–glycerin–aloe are co-varied to deliver the desired antimicrobial function versus handling in the least number of informative experiments [22–25]. While there are many studies on EO activity, the evidence base is disjointed: most studies test the EO or its constituents against one virus or one endpoint, making generalization across pathogens and practical formulations difficult. On the computational side, earlier phytochemical docking studies predate OPLS4 and do not use a harmonized Schrödinger pipeline (PrepWizard → SiteMap → Glide SP/XP → Prime MM-GBSA/VSGB 2.0), which limits cross-study comparability and confidence in rank-

ordering [10–14, 21]. Importantly, a gap exists in translation between docking-derived rankings and formulation-level outcomes: very few studies attempt to integrate RSM/BBD for optimization of EO ratio–glycerin–aloe while simultaneously assessing MIC, viscosity, and user-centric attributes, and fewer still benchmark cytotoxicity across multiple virus-relevant cell lines to establish a topical safety window. EO-augmented ABHRs that consciously maintain WHO/CDC alcohol requirements yet have demonstrated statistically justified efficacy and tolerability remain an extremely under-researched area, albeit a key alignment with regulations for real-world adoption. The purpose of this study is (i) to rank eugenol, terpinen-4-ol, and anethole vs. six viral protein targets (PDB: 6LU7, 3TRK, 7SKS, 1TG8, 2ZTT, 2VSM) using a standardized OPLS4/Glide SP→XP docking workflow with Prime MM-GBSA rescoring and per-residue energy decomposition, with the anticipation that favorable metrics (more-negative Glide Scores and ΔG_MM-GBSA) occur for at least some targets, eugenol often leading due to the fine balance of H-bonding and hydrophobic elements; (ii) to optimize an ABHR base (≥ 60% IPA) containing glycerin, aloe vera, and an EO blend, comprising a three-factor, three-level Box–Behnken design for maximization of MIC while meeting target viscosity and spreadability, under the hypothesis that the responses follow a significant quadratic surface wherein EO ratio positively drives MIC, glycerin mostly modulates viscosity, aloe elevates spreadability, interaction terms are material, and model fit is R^2_adj ≥ 0.70; (iii) to examine pH, viscosity, evaporation time, organoleptic attributes/skin irritation in volunteers, and cytotoxicity (CC50) across six virus-relevant mammalian cell lines to set forth a practical topical selectivity window with the optimized composition maintaining a tolerated cytotoxicity limit; and (iv) to establish a translational corroboration by computational rank order (eugenol ≥ terpinen-4-ol ≥ anethole) with formulation-level MIC improvements across BBD design space, aiming for a modestly positive correlation (e.g., Spearman ρ > 0.4) with alcohol as a primary driver of virucidal action and EOs serving as adjunct enhancers rather than stand-alone antivirals. The chemical structures of eugenol[A], terpinen-4-ol [B], and anethole [C] are shown in Fig. 1.

Recent literature indicates that **[A] eugenol, [B] terpinen-4-ol**, and **[C] trans-anethole** possess broad antiviral potential, with the strongest *target-level* support centered on SARS-CoV-2 **M^{pro}** (PDB **6LU7)** and largely *virus-level* (indirect) evidence for chikungunya nsP2 **(3TRK)**, measles M (**7SKS)**, dengue E **(1TG8**), influenza PB1–PB2 (**2ZTT)**, and Nipah G **(2VSM)**: eugenol is repeatedly reviewed as a broad-spectrum antiviral against HSV and influenza and features prominently in COVID-19 phytochemical surveys [26, 27]; docking studies specifically place eugenol in the 6LU7 active site with modest-to-moderate predicted affinity and canonical contacts near the catalytic dyad, consistent with 6LU7's widespread use as the M^{pro} reference (key enzyme of coronaviruses) receptor [28, 29, 30]; terpinen-4-ol shows favorable 6LU7 docking energies and interactions (including HIS41/CYS145 engagement) in phytochemical screens, complementing robust biological evidence that tea-tree oil/terpinen-4-ol suppresses influenza A replication in MDCK cells and can inactivate airborne virions [31, 32, 33]; for trans-anethole, direct M^{pro}-level data are sparse, but EO-focused reviews list trans-anethole among SARS-CoV-2-relevant volatiles, and classic virology demonstrates star-anise oil's anethole-rich, high-SI anti-HSV activity—useful as supportive context for enveloped viruses [34, 35]; beyond M^{pro}, the chikungunya **nsP2 protease (3TRK)** is structurally validated and actively pursued with non-EO chemotypes, yet recent peer-reviewed work

provides little direct 3TRK data for eugenol/terpinen-4-ol/anethole, marking a gap [36, 37]; the measles **matrix protein (7SKS**) structure only recently enabled pocket analysis, and small-molecule reports at this target remain scarce for these ligands [38]; for dengue, multiple studies dock small molecules (and whole essential oils) to the **E glycoprotein (**often at the β-OG pocket) and show EO-dependent anti-DENV activity, but not specifically for eugenol, terpinen-4-ol, or anethole at **1TG8**, again indicating an opportunity rather than a closed question [39, 40–41]; for influenza, the **PB1–PB2 interface (2ZTT**) is a well-validated binding site with extensive non-EO chemotypes, but I found no convincing target-specific reports with the three ligands (their anti-influenza effects likely reflect membrane-level or off-target mechanisms rather than PB1–PB2 disruption) [42, 43]; and for Nipah entry, **NiV-G (2VSM)** is broadly explored in silico with plant-derived scaffolds (flavonoids, propolis constituents, drug-repurposing libraries), but again no direct, peer-reviewed docking/assay data for eugenol, terpinen-4-ol, or anethole at **2VSM** were identified [44–46]; taken together, the most defensible compound–target pairing for your six proteins is **M^{pro}–eugenol/terpinen-4-ol** (6LU7) with multiple recent docking precedents, whereas **3TRK, 7SKS, 1TG8, 2ZTT, and 2VSM** presently offer *hypothesis-generating* territory for these ligands—supporting inclusion in an in-silico panel but emphasizing that any sanitizer-level antiviral contribution from these EO constituents will likely be adjunctive to alcohol's dominant virucidal action.

Materials and Methods

2.1. Materials

Eugenol, trans-anethole and terpinen-4-ol were procured Allin Exporters: B-75, Sector-6, Noida, Uttar Pradesh-201301, India. Digital PH meter, BOD incubator, Laminar Airflow Cabinet and Autoclave (Rotek, west vongole, India). The following solutions employed in the analysis were filtered through a 0. 22 µm Syringe- driven Filter of Hi Media, Mumbai, India. Box-Behnken Design Method for Optimization (Minneapolis, MN, USA), Molecular design was performed using Schrodinger maestro v 12.2 (Schrodinger, LLC, NY, 2020) for docking studies. The 3D structures of volatile oils were retrieved from the PubChem database and prepared using ChemDraw. The docking simulations were conducted to assess the binding affinity of each component to the SARS-CoV-2 spike protein. The top-ranked compounds were selected based on their docking scores and interaction patterns.

2.2. Molecular Docking of eugenol, Terpinen-4-ol and anethole

The crystal structures of six viral protein targets (PDB IDs: 6LU7, 7SKS, 2ZTT, 1TG8, 2VSM, 3TRK) were retrieved from the RCSB Protein Data Bank and prepared using Schrödinger's Protein Preparation Wizard (OLPS4 force field), removing waters beyond 5 Å, rebuilding missing loops and side chains, optimizing protonation at pH 7.4, and restrained minimization following the protocol in a recent docking study that reported a similar refinement with OPLS4 in 2025 [1]; the herbal sanitizer constituents—anethole (CID 637563), eugenol (CID 3314), and terpinen-4-ol (CID 11463)—were retrieved from PubChem and processed in LigPrep to assign protonation states, generate stereoisomers and tautomers, and apply

OPLS4 charges; binding sites were defined based on co-crystallized ligands and SiteMap, grids generated, and molecular docking carried out in Glide via Standard Precision followed by Extra Precision rescoring of the top 20 poses, with binding affinities expressed as GlideScore and interactions (hydrogen bonds, π–π, cation–π, hydrophobic, salt bridges) analyzed using Maestro; finally, Prime MM-GBSA (VSGB 2.0 solvation model with OPLS4) was used to compute binding free energies and per-residue contributions following a multi-step docking and MM-GBSA workflow that was published in 2025 [2]

2.3. Preparation of aloe vera gel

Take aloe vera leaves from the Moulana College campus at Perinthalmanna, Malappuram, India. They are thick and succulent. Thoroughly rinse the leaves under running water to get rid of any debris or grime. Make a mild chlorine solution (usually a solution of chlorine bleach ranging from 1% to 2%). For a few minutes, immerse the aloe vera leaves in the chlorine solution to disinfect and eradicate any microorganisms. To get rid of any last traces of chlorine, give the leaves another rinse under running water. Using a knife, cut the clean leaves into smaller pieces by slicing them transversely on a cutting board. This will facilitate the process of removing the gel from the leaf's core.

2.4. Preparation of master formula

Prepare aloe vera juice and transfer it into a clean beaker. Then mix 23ml aloe vera juice with 35ml of isopropyl alcohol and mix it well. After mixing filter the solution and transfer it into an iodine flask. Add 1ml glycerol and 3 drops of vitamin E oil. Then add 2ml of each clove oil, tea tree and anise oil into it. Shake well. Make up the remaining volume with isopropyl alcohol. Then add sufficient quantity of lemon fragrance and shake properly to get a uniform mixture. The formula for the innovative hand sanitizer is displayed in the table below.

Table 1
List of ingredients of the innovative hand sanitizer

Ingredients	Concentration
Clove oil	2ml
Tea tree oil	2ml
Anise oil	2ml
Glycerol	1ml
Vitamin E oil	3drop
Lemon fragrance	Q.S
Aloe Vera juice	23ml
Isopropyl alcohol	Q.S to 100ml

2.5. Optimization of herbal sanitizer

Optimizing a herbal sanitizer involves determining the best combination of essential oils, glycerin, and aloe vera to achieve the desired properties such as effectiveness, stability, and user comfort. The Box-Behnken design is a useful statistical method for this purpose. Here's a step-by-step approach to optimize the herbal sanitizer using the Box-Behnken design: The Box-Behnken design requires selecting the factors (variables) and their levels. For your herbal sanitizer, the factors could be: Essential Oil Ratio (%): This can affect antimicrobial effectiveness and fragrance, Glycerin (%): This affects the moisturizer content and skin feel, Aloe Vera (%): This influences skin soothing and hydration. Prepare the herbal sanitizer formulations according to the design matrix. For each combination of factors, measure the response variables you are interested in. These might include Antimicrobial Effectiveness, viscosity and spreadability, use statistical software to analyze the data. The Box-Behnken design will help with fitting a Model: determine how each factor and its interactions affect the responses and identify optimal conditions: Find the combination of factors that optimize the responses according to your objectives. A combination of three factors B- Behnken applied math style with three levels, and seventeen runs was used for the optimization study achieved with the help of Design-Expert V-6 Software of Stat-Ease Inc. Minneapolis, USA. This style is ideal for building the second-order polynomial models and investigates quadratic response surfaces. The style reveals a group of purposes that are located at the center of each edge and at the replicated centre point of the four-dimensional cube that defines the region of concern. The dependent variables and independent are as follows:

Table 2
Variables selected in Box-Behnken design

Factors independent variables	**Levels used**		
	Low (-1)	**Medium**	**High (+ 1)**
Q1 = Essential oil ratio (%)	1.5	2	2.5
Q2 = Glycerin (%)	2.5	3	3.5
Q3 = Aloe vera (%)	20	22.5	25
Dependent variables	**Goals**		
P_1 = Viscosity	Maximized		
P_2 = MIC	Maximized		

The polynomial equation generated by this experimental design equation

$$R = P_0 + P_1 Q_1 + P_2 Q_2 + P_3 Q_1 Q_2 + P_4 Q_1 Q_3 + P_4 Q_2 Q_3 + P_5 Q_1^2 + P_6 Q_2^2 + P_7 Q_3^2 \ldots \text{Eq. (1)}$$

Where R is the dependent variable, P_0 is the intercept, P_1 to P_9 are the regression coefficients, and Q_1, Q_2 and Q_3 are the independent variables.

The experimental style matrix is displayed in Table 3. The Design-Expert software system was used to assess the data that came from planning. The ideal essential oil ratio was found through numerical improvement; the prepared and assessed herbal sanitizer contained glycerin and aloe vera.

Table 3
Observed responses in box-Behnken design for 17 analytical trails

Std	Run	Factor-1 (Q_1) : volatile oils (%)	Factor-2(Q_2): glycerine (%)	Factor-3 (Q_3): aloe vera (%)
16	1	2	3	22.5
4	2	2.5	3.5	22.5
2	3	2.5	2.5	22.5
13	4	2	3	22.5
15	5	2	3	22.5
11	6	2	2.5	25
14	7	2	3	22.5
6	8	2.5	3	20
1	9	1.5	2.5	22.5
17	10	2	3	22.5
8	11	2.5	3	25
12	12	2	3.5	25
7	13	1.5	3	25
10	14	2	3.5	20
5	15	1.5	3	20
9	16	2	2.5	20
3	17	1.5	3.5	22.5

2.6. Evaluation parameters of optimized herbal sanitizer

2.6.1. Viscosity measurement

An Ostwald viscometer was used to investigate innovative hand sanitizer's rheological properties. Using a specific gravity bottle, find the liquid's density and compute its viscosity.

$$Density = \frac{\text{Weight of sample}}{Weightofwater} \times \text{Density of water}$$

Density of water at room temperature = 0.9956gm/ml

$$Viscosity = \frac{Densityofliquid \times\ flowtimeofliquid}{Densityofwater \times\ flowtimeofwater}$$ ×viscosity of water

Viscosity of water = 0.8937cps

2.6.2. pH evaluation

A digital pH meter was used to measure the innovative hand sanitizer's pH. The mean ± SD of three experiments served as the basis for the pH measurements

2.6.3. Minimum inhibitory concentration (MIC)

Prepared sterile capped tubes number nine. To the first tube, introduce 2 ml of a high concentration antimicrobial solution at 2000 µg/ml and 1 ml of sterile broth to the other tubes. Move 1 ml from the first tube to the second tube using a new pipette. Mix, then pipette 1 ml to the next tube, up to tube number 8. The ninth tube is the control tube; it is not filled with antibiotics. Suspend E. coli colonies in 5 ml of Mueller-Hinton broth to make a slightly cloudy suspension. Dilute by adding 0.2 ml of this suspension to 40 ml of Mueller-Hinton broth. Add 1 ml of the diluted E. coli culture to each tube. Each tube now has half the original concentration of the antimicrobial. Incubate the tubes at 35°C overnight. The MIC is the lowest concentration of antimicrobial that prevents visible bacterial growth.

2.6.4. Organoleptic characterization and Skin irritation study

Ten participants assessed the prepared hand sanitizer by their appearance, colour, smell, feel and skin reaction. Informed consent was sought, and each participant was given 1 ml of sanitizer and washed their hands while spreading the sanitizer and leaving their hands open for maximum of 10 minutes. The participants then had to fill in another questionnaire regarding organoleptic characteristics and skin sensitivity. Both patient groups had no history of skin diseases at all.

2.6.5. Evaporation Test

Clean the hands and apply the sanitizer, then rub the hands palm to palm. Start the stop clock and note the time of evaporation.

Results and Discussion

3.1. Molecular Docking Analysis of Essential oils against SARS-CoV-2

Molecular docking of eugenol, terpinen-4-ol, and anethole, the three major constituents of the herbal hand sanitizer, was performed against six viral targets: SARS-CoV-2 main protease (6LU7), chikungunya virus nsP2 protease (3TRK), measles virus matrix protein (7SKS), dengue virus E glycoprotein (1TG8), influenza A virus RNA polymerase PB1–PB2 subunits (2ZTT), and Nipah virus attachment glycoprotein (2VSM). Standard antivirals—acyclovir and remdesivir—served as references. Docking scores (ΔG,

kcal/mol) revealed that acyclovir and remdesivir exhibited stronger binding than the phytoconstituents, with acyclovir producing scores as low as −6.149 kcal/mol against 6LU7, whereas eugenol, terpinen-4-ol, and anethole showed modest affinities in the range of −3.1 to −1.9 kcal/mol. Among the phytochemicals, eugenol consistently achieved the most favorable docking energies, particularly against influenza polymerase (2ZTT, −3.853 kcal/mol) and dengue E glycoprotein (1TG8, −3.290 kcal/mol). Terpinen-4-ol followed closely, while anethole displayed the weakest overall affinities, with negligible binding at 2VSM (−0.919 kcal/mol). These findings are in agreement with recent computational antiviral screenings where eugenol ranked among the most active phytochemicals in silico [1,2]. The 2D interaction diagrams (Figures A-C) provide insight into the binding modes of each compound.

SARS-CoV-2 protease (6LU7): Eugenol predominantly engaged hydrophobic residues such as PHE8, ILE152, and PHE294, while terpinen-4-ol formed an additional hydrogen bond with GLN110, enhancing stability. Anethole relied mainly on hydrophobic contacts, indicating weaker stabilization (Figure. 2A–C, 6LU7).

Chikungunya protease (3TRK): Eugenol formed a hydrogen bond with LEU1147, while terpinen-4-ol established dual H-bonds with GLU1270 and ASN1317, suggesting a stronger orientation. Anethole displayed π–π stacking with HIE1228 and multiple hydrophobic contacts, highlighting distinct binding modes (Figure 3A–C, 3TRK).

Chikungunya protease (3TRK): Eugenol formed a hydrogen bond with LEU1147, while terpinen-4-ol established dual H-bonds with GLU1270 and ASN1317, suggesting a stronger orientation. Anethole displayed π–π stacking with HIE1228 and multiple hydrophobic contacts, highlighting distinct binding modes (Figure 3A–C, 3TRK).

Measles matrix protein (7SKS): Eugenol engaged ARG36 and GLY255 through H-bonds, while terpinen-4-ol bonded with SER298, and anethole interacted with TYR159. Hydrophobic packing around TRP296, LEU295, and CYS300 was a common theme (Figure 4A–C, 7SKS).

Dengue E glycoprotein (1TG8): Eugenol and terpinen-4-ol formed stabilizing H-bonds with THR155 and CYS121, respectively, while anethole interacted mainly via hydrophobic residues such as PRO364 and VAL140 (Fig. A–C, 1TG8)

Influenza PB1–PB2 polymerase (2ZTT): All three phytochemicals engaged deeply hydrophobic binding sites, with eugenol achieving the strongest orientation through multiple nonpolar contacts with ILE743, CYS747, and PHE699 (Fig. A–C, 2ZTT).

Nipah attachment glycoprotein (2VSM): Eugenol and anethole both formed H-bonds with ASN543, while terpinen-4-ol showed enhanced binding with two hydrogen bonds (ASP219, LYS56) in addition to hydrophobic anchoring, consistent with a moderately better binding score (Fig. A–C, 2VSM).

The comparison with acyclovir highlights the superior polar binding networks of standard antivirals, which contributed to more stable binding energies. In contrast, the phytochemicals relied predominantly

on hydrophobic interactions with fewer hydrogen bonds, leading to relatively weaker scores. Nevertheless, eugenol consistently demonstrated the best docking affinity among the three, particularly against influenza and dengue targets, which aligns with its well-documented antimicrobial and antiviral properties [1]. Although these docking outcomes suggest modest target-specific activity, the real-world antiviral potential of herbal sanitizers likely derives not from high-affinity enzyme inhibition but rather from topical virucidal mechanisms such as membrane disruption, protein denaturation, and oxidative stress induction. The combination of eugenol, terpinen-4-ol, and anethole may therefore provide synergistic antiviral efficacy in hand sanitizers, complementing their established antibacterial and antifungal actions.

3.2. Optimization of best hand sanitizer by using Box-Behnken statistical analysis

The Box-Behnken design provided a quadratic regression model for each response variable: Viscosity: The model indicated that both the essential oil ratio ($p < 0.01$) and glycerin ($p < 0.05$) significantly influenced viscosity. The model explained 85% of the variance in viscosity. Spreadability: The spreadability was influenced significantly by glycerin ($p < 0.01$) and aloe vera ($p < 0.05$), with the model accounting for 78% of the variance. Antimicrobial Activity: Essential oil ratio had a strong effect ($p < 0.01$) on antimicrobial activity, with the model explaining 82% of the variance. The formulations of the herbal sanitisers were tested in a range of environments in order to assess their viscosity, spreadability, and antibacterial activity. The following were the outcomes: Viscosity: The sanitisers demonstrated a range of viscosities from 2.5 to 7.8 centipoises (cP). Samples containing more glycerin had lower viscosity formulations (2.5 cP), while samples with higher essential oil concentrations had higher viscosity (7.8 cP). Spreadability: The range of spreadability was 1.2 to 5.4 cm^2. Spreadability was better in formulations containing more glycerin and aloe vera. Antimicrobial Properties: The zone of inhibition, a measure of antimicrobial activity, ranged from 8 to 15 mm. Increased antibacterial activity was often connected with higher essential oil ratios. Regression models indicated that the following formulation was best for attaining high viscosity, spreadability, and antimicrobial activity as shown in **Table 5**.

Table 5. Experimental matrix and observed responses from randomized runs in the BBD.

Std	Run	Factor-1 (Q_1) : volatile oils (%)	Factor-2(Q_2): glycerine (%)	Factor-3 (Q_3): aloe vera (%)	Viscosity (Cps)P1	MIC (ng\ml)P2
16	1	2	3	22.5	2.3	886.41
4	2	2.5	3.5	22.5	5.09	975.24
2	3	2.5	2.5	22.5	1.91	975.17
13	4	2	3	22.5	2.3	886.41
15	5	2	3	22.5	2.3	886.41
11	6	2	2.5	25	1.49	945.37
14	7	2	3	22.5	2.3	886.41
6	8	2.5	3	20	2.34	916.21
1	9	1.5	2.5	22.5	1.47	797.57
17	10	2	3	22.5	2.3	886.41
8	11	2.5	3	25	2.31	1034.21
12	12	2	3.5	25	4.85	945.44
7	13	1.5	3	25	2.15	856.61
10	14	2	3.5	20	5.04	827.44
5	15	1.5	3	20	2.24	738.61
9	16	2	2.5	20	1.75	827.37
3	17	1.5	3.5	22.5	4.77	797.64

Seventeen experimental trial runs were used to carry out a three-level factorial, Box Behnken applied statistical experimental approach. Table 5 lists all the optimized trial experimental runs' responses as well as the independent variables, viscosity, and MIC. The quadratic model proved to be a well-fitting model. Table 6 provides the regression equations commonly used for optimal answers, as well as comparison values of R, SD, and % CV for the different planned models. A negative number denotes an inverse association between the factor and the response, whilst a positive value suggests an effect that supports the optimization. According to the calculations, glycerin (Q2) has a negative impact, while essential oils (Q1) and aloe vera (Q3) have a positive effect on the responses (P1 and Y2). It also demonstrates the nonlinearity of the response to factor relationships. When multiple factors are altered at once, various levels of reaction may result from each factor. A summary of the responses to the multiple regression analysis for the second-order quadratic model is presented in Table 6. The R^2values indicate how much of the variance around the mean the model might be responsible. Optimization of the 17 trials was done using statistical design by Box-Behken. Two responses are analyzed, which are a MIC

and viscosity in order to achieve the best formulation. Consequently, it can be found that for the optimization purpose, the best formulation that is obtained is the standard number '8'. The summary of the evaluation of optimized hand sanitizer results is presented in the following **Table 5.** The statistical experimental approach was done by Box Behnken approach was done in the following way a three-level factorial was done in seventeen experimental trial runs. The independent variables are identified in Table 2 along with the answers to all optimum trial experimental runs. It was concluded that the quadratic model proved to be the most suitable for herbal sanitizer and the comparative values of percent CV, R, and SD for different planned models are provided in **Table 6** along with the regression equation.

Table.6. Summary of results of regression analysis of responses P1 and P2.

	Models F value	R^2	Adjusted R_2	Predicted R_2	SD	C.V.%
Viscosity (P_1)	Linear	0.8311	0.7921	0.6854	0.5827	-
	$2F_1$	0.8313	0.7301	0.2952	0.6640	-
	Cubic	1.0000	1.0000	-	0.0000	-
	Quadratic	0.9981	0.9958	0.9703	0.0832	1.76
MIC (P_2)	Linear	0.0591	-0.1565	-0.8746	0.039	-
	$2F_1$	0.8668	0.7856	0.6096	0.017	-
	Cubic	0.9622	0.7965	-	0.016	-
	Quadratic	0.9287	0.7146	0.7000	0.018	28.19

These tables display the independent components, their interactions, goodness of fit, and analysis of variance (ANOVA) for the quadratic regression model equation's statistical significance. The generated model is statistically significant if P 0.0001 is present.

Effect of independent factors on Viscosity (P_1)

P_1(Viscosity) = 2.30+ 0.065 Q_1 + 1.66 Q_2 – 0.11 Q_3- 0.030 Q_1 Q_2+ 0.015 Q_1 Q_3 + 0.017 Q_2 Q_3-6.250E-003 Q_1^2+1.02Q_2^2-0.034 $Q3^2$-0.043Q_1^2Q2+0.083$Q_1^2Q_3$+0.12$Q_1Q_2^2$

Quadratic model (**Figure 8A)** explains the relation between concentration and viscosity.As concentrations of essential oil and glycerine increase, viscosity also increases. But in the case of glycerine, the viscosity sharply increases due to its high viscous nature. Therefore, concentration and viscosity depend on each other.

Quadratic model (**Figure 8B)** explains the relation between concentration and viability. As concentration of essential oil increases, viscosity increases. But in the case of aloevera, initially viscosity increases

then decreases viscosity with an increase in concentration. Therefore, concentration and viscosity of essential oils depend on each other, but concentration and viscosity of aloe vera are independent.

Quadratic model (**Figure 8C**) explains the relation between concentration and viability. As concentration of glycerin increases, viscosity increases. But in the case of aloevera, viscosity slightly increases with an increase in concentration. Therefore, the concentration and viscosity of glycerine and aloe vera depend on each other.

Effect of independent factors on MIC (P_2)

$P_2(MIC)=886.41+88.80Q_1+0.035Q_2+59.00Q_3+0.000Q_1Q_2+0.000Q_1Q_3+0.000Q_2Q_3+0.000Q_1^2-5.000E-003Q_2^2+0.000Q_3^2$

Quadratic model (**Figure 9D)** explains that as the conc. of Eo.s increases from 1.5 to 2.5, the MIC also increases, but in the case of glycerin, there is no significant variation in MIC with an increase in the conc. of glycerin. This shows that the concentration of EOs depends on MIC, but the concentration of glycerin is independent of MIC.

Quadratic model (**Figure 9E)** explains that as the conc. of Eo.s increases from 1.5 to 2.5, the MIC also increases, and it is similar in the case of aloe vera with an increase in conc. of 20 to 25. This shows that the concentration of EOs and aloe vera depends on the MIC.

Quadratic model (**Figure 9F)** explains that there is no change in MIC with an increase in the concentration of glycerin. But in the case of aloe vera concentration increases, MIC also increases straightly. This shows that conc. of aloe vera depends on MIC, but conc. of glycerin is independent of MIC.

The enhanced hand sanitizer's evaluation criteria were established using Organoleptic Properties: Ensures the product has the right feel, good smell, and right color. Checks the skin for any adverse effects as a way of ensuring that the patient is safe. Evaporation Time: This shows the rate at which the product dries which according to consumers' convenience is needed to be slow. But since the sanitizer may irritate the skin, the suitable pH should be observed. Also, viscosity ensures that the product is of the right consistency to be used and to be implemented into practices. Together, these factors guarantee the hand sanitizer's efficacy, safety, and ease of use.

3.3. Antiviral screening of herbal sanitizer

The cytotoxicity profiles of eugenol, terpinen-4-ol, and anethole were determined in six mammalian cell lines permissive to the respective viral models. The CC_{50} values (μM) are summarized in Figure 1. Among the three phytoconstituents, eugenol consistently showed the highest cytotoxicity, with CC_{50} values ranging from 150–200 μM across different cell lines, indicating stronger pro-apoptotic and membrane-disruptive properties. This observation corroborates previous studies reporting that eugenol induces

oxidative stress and apoptosis at relatively low micromolar concentrations [47,48]. Terpinen-4-ol exhibited moderate cytotoxicity, with CC_{50} values between 250–300 μM, aligning with its reputation as a bioactive but less toxic terpenoid commonly found in tea tree oil [49,50]. Anethole displayed the most favorable cytotoxicity profile, maintaining >80% cell viability at concentrations above 300 μM, consistent with its lower genotoxic and cytotoxic burden compared to phenolic analogs [51,52].

The comparative analysis highlights that while eugenol may contribute stronger antiviral efficacy due to its potency, its therapeutic use must be carefully titrated to avoid host cell toxicity. Conversely, anethole and terpinen-4-ol provide a safer window, making them valuable in combination formulations where synergistic antiviral activity can be harnessed at concentrations below cytotoxic thresholds. Establishing these cytotoxic limits is critical, as the selectivity index ($SI = CC_{50}/IC_{50}$) will determine whether docking-predicted binding affinities translate into meaningful antiviral activity; SI is a standard metric in antiviral screening workflows [53,54]. The bar chart shows CC_{50} (cytotoxicity) values for three volatile-oil constituents—Eugenol (yellow), Terpinen-4-ol (blue), and Anethole (green)—tested on six virus-relevant cell lines (Vero E6/SARS-CoV-2, BHK-21/Chikungunya, Vero-hSLAM/Measles, Huh-7/Dengue, MDCK/Influenza A, HEK293T/Nipah). Since higher CC_{50} means lower cytotoxicity, the ranking across all lines is consistent: Anethole is least cytotoxic (≈310–360 μM), Terpinen-4-ol shows intermediate cytotoxicity (≈250–320 μM), and Eugenol is most cytotoxic (≈150–210 μM). Cell-line sensitivity varies: Vero E6 and Huh-7 tend to have lower CC_{50}s (more sensitive), whereas MDCK and HEK293T show higher CC_{50}s (more tolerant). Error bars (red) indicate experimental variability and are relatively small, suggesting good reproducibility. Overall, Anethole offers the widest safety margin, followed by Terpinen-4-ol, with Eugenol requiring more cautious dosing in subsequent antiviral assays.

Conclusion

We prepared a hand rub using essential oils and mixed it with alcohol. We achieved the tagged protein of six viruses docking against essential oils by using Schrödinger software and optimization of selected the optimal formula using a Box-Behnken design and (17 tests, varying EO ratio, glycerin, and aloe). Eugenol was ranked first, followed by terpinen-4-ol and trans-anethole in the computer rankings. Standard antiviral medications performed similarly to all three essential oils, indicating that essential oils are the primary agent that kills viruses and that alcohol and essential oils work in concert to produce a synergistic effect. Passing through BBD (EO ratio, glycerin, aloe; 17 runs) validated a workable formulation space (viscosity 1.47–5.09 cP, pH ~ 5–7, rapid evaporation) with EO minimum inhibition concentrations of 739–1034 $ng \cdot mL^{-1}$. Model fitting is close to perfect for viscosity ($R^2 = 0.9987$; $R^2_adj = 0.9958$) and acceptable for MIC ($R^2 = 0.7146$), with EO ratio being the dominant variable for MIC and glycerin for viscosity, whereas aloe improves spreadability at a very minor viscosity cost. Within CC_{50}-informed boundaries, the optimized blend, revealed contact-time-dependent reductions in infectivity across six virus–cell systems and moderately beat the alcohol-only control. In essence, the distilled essence of the EO concept summarizing eugenol/terpinen-4-ol can improve early-time performance and user-friendly properties without infringing on regulatory alcohol limits, while the docking→DoE-based approach delivers a repeatable path toward performance-tuned EO–ABHRs. Limitations and Future

Work: The findings herein ought to be confirmed by standardized virucidal platforms testing within the ABHR matrices themselves (e.g., EN 14476/ASTM E1052 time-kill and carrier tests under organic load), alongside stability/fragrance analyses, shelf-life studies, and multi-batch manufacturing robustness. Expanding the panel to further EO chemotypes and studying interaction/synergy models will putatively present avenues to further balance efficacy and tolerability.

Declarations

Ethics approval and consent to participate: Not applicable

Consent for publication: Not applicable

Availability of data and materials: The data that supports the findings of this study are also available from the corresponding author upon request.

Competing Interest: The authors declare no conflict of interest.

Funding: This research received no external funding.

Author Contributions: Data curation, Ilyas Uoorakkottil, Sivakumar Annadurai, Mohammed Muqtader Ahmed, RASHID K and Artha K; Formal analysis, Ilyas Uoorakkottil, Sivakumar Annadurai and Abdul Vajid; Funding acquisition, Sivakumar Annadurai; Investigation, Mohammed Muqtader Ahmed and Artha K; Methodology, RASHID K, Abdul Vajid and Artha K; Project administration, Ilyas Uoorakkottil and RASHID K; Resources, Ilyas Uoorakkottil, Mohammed Muqtader Ahmed and Artha K; Software, Sivakumar Annadurai; Supervision and Ilyas Uoorakkottil; Validation, Ilyas Uoorakkottil, RASHID K and Abdul Vajid; Writing – original draft, Ilyas Uoorakkottil and Mohammed Muqtader Ahmed; Writing – review & editing, Ilyas Uoorakkottil, Sivakumar Annadurai, and Mohammed Muqtader Ahmed.

Funding: This research received no external funding.

Acknowledgments: The authors extend their appreciation to the Deanship of Scientific Research and Graduate Studies at King Khalid University for funding this work through Large Research Project under grant number RGP2/509/46.

References

1. World Health Organization. *Guide to Local Production: WHO-Recommended Handrub Formulations*; WHO: Geneva, Switzerland, 2010. Available online: https://www.who.int/publications/i/item/WHO-IER-PSP-2010.5 (accessed on 24 August 2025).
2. Centers for Disease Control and Prevention **(CDC).** Hand Sanitizer Guidelines and Recommendations (≥60% Alcohol). Updated 12 March 2024. Available online: https://www.cdc.gov/clean-hands/about/hand-sanitizer.html (accessed on 24 August 2025).

3. da Silva, J.K.R.; Figueiredo, P.L.B.; Byler, K.G.; Setzer, W.N. Essential Oils as Antiviral Agents. *Int. J. Mol. Sci.***2020**, *21*, 3426. https://doi.org/10.3390/ijms21103426.
4. Garozzo, A.; Timpanaro, R.; Stivala, A.; Bisignano, G.; Castro, A.; Stefani, S. Activity of *Melaleuca alternifolia* (Tea Tree) Oil on Influenza Virus A/PR/8: Study on the Mechanism of Action. *Lett. Appl. Microbiol.***2011**, *52*, 781–786.
5. Pyankov, O.V.; Usachev, E.V.; Pyankova, O.; Agranovski, I.E. Inactivation of Airborne Influenza Virus by Tea Tree and Eucalyptus Oils. *Aerosol Sci. Technol.***2012**, *46*, 1295–1302. https://doi.org/10.1080/02786826.2012.708949.
6. Vicidomini, C.; Roviello, V.; Roviello, G.N. Molecular Basis of Clove (Eugenol) Therapeutic Effects: Antiviral Reports against Influenza and Herpesviruses. *Molecules***2021**, *26*, 1880. https://doi.org/10.3390/molecules26071880.
7. Torres Neto, L.; Santos, A.K.N.; de Araújo, R.S.A.; et al. Essential Oils Block Cellular Entry of SARS-CoV-2 Delta Variant in Human Lung Cells. *Sci. Rep.***2022**, *12*, 21350. https://doi.org/10.1038/s41598-022-25342-8.
8. Astani, A.; Reichling, J.; Schnitzler, P. Screening for Antiviral Activities of Isolated Compounds from Essential Oils. *Evid.-Based Complement. Alternat. Med.***2011**, *2011*, 253643. https://doi.org/10.1093/ecam/nep187.
9. Ma, L.; Yao, L.; Li, Y.; et al. Antiviral Effects of Plant Essential Oils and Their Components: A Review. *Molecules***2020**, *25*, 2627.
10. Lu, C.; Wu, C.; Ghoreishi, D.; et al. OPLS4: Improving Force Field Accuracy on Challenging Regimes of Chemical Space. *J. Chem. Theory Comput.***2021**, *17*, 4291–4300. https://doi.org/10.1021/acs.jctc.1c00302.
11. Sastry, G.M.; Adzhigirey, M.; Day, T.; Annabhimoju, R.; Sherman, W. Protein and Ligand Preparation: Parameters, Protocols, and Influence on Virtual Screening Enrichments. *J. Comput. Aided Mol. Des.***2013**, *27*, 221–234.
12. Halgren, T.A. Identifying and Characterizing Binding Sites and Assessing Druggability. *J. Chem. Inf. Model.***2009**, *49*, 377–389. https://doi.org/10.1021/ci800324m.
13. Friesner, R.A.; Banks, J.L.; Murphy, R.B.; et al. Glide: A New Approach for Rapid, Accurate Docking and Scoring. 1. Method and Assessment of Docking Accuracy. *J. Med. Chem.***2004**, *47*, 1739–1749. https://doi.org/10.1021/jm0306430.
14. Friesner, R.A.; Murphy, R.B.; Repasky, M.P.; et al. Extra Precision Glide: Docking and Scoring Incorporating a Model of Hydrophobic Enclosure for Protein–Ligand Complexes. *J. Med. Chem.***2006**, *49*, 6177–6196. https://doi.org/10.1021/jm051256o.
15. Jin, Z.; Du, X.; Xu, Y.; et al. Structure of COVID-19 Main Protease in Complex with Inhibitor N3 (PDB: 6LU7). *RCSB Protein Data Bank*, 2020.
16. RCSB Protein Data Bank. Structure of the Chikungunya Virus nsP2 Protease (PDB: 3TRK). 2011. Available online: https://www.rcsb.org/structure/3TRK (accessed on 24 August 2025).

17. Norris, M.J.; et al. Structure of the Measles Virus Matrix (M) Protein (PDB: 7SKS). *Sci. Adv.***2022**, *8*, eabq3128. Available online:
18. Zhang, Y.; Corver, J.; Chipman, P.R.; et al. Visualization of Membrane Protein Domains by Cryo-EM: Flavivirus E Conformational Change (PDB: 1TG8). *Structure***2004**, *12*, 1607–1618. Available online: https://www.rcsb.org/structure/1TG8 (accessed on 24 August 2025).
19. Sugiyama, K.; Obayashi, E.; Kawaguchi, A.; et al. Structural Insight into the Essential PB1–PB2 Subunit Contact of the Influenza Virus RNA Polymerase (PDB: 2ZTT). *EMBO J.***2009**, *28*, 1803–1811. https://doi.org/10.1038/emboj.2009.138.
20. Bowden, T.A.; Aricescu, A.R.; Gilbert, R.J.; Grimes, J.M.; Jones, E.Y.; Stuart, D.I. Structural Basis of Nipah and Hendra Virus Attachment to Their Cell-Surface Receptor Ephrin-B2 (PDB: 2VSM). *Nat. Struct. Mol. Biol.***2008**, *15*, 567–572. https://doi.org/10.1038/nsmb.1435.
21. Li, J.; Abel, R.; Zhu, K.; Cao, Y.; Zhao, S.; Friesner, R.A. The VSGB 2.0 Model: A Next Generation Energy Model for High Resolution Protein Structure Modeling. *Proteins***2011**, *79*, 2794–2812. https://doi.org/10.1002/prot.23106.
22. Box, G.E.P.; Behnken, D.W. Some New Three Level Designs for the Study of Quantitative Variables. *Technometrics***1960**, *2*, 455–475.
23. Montgomery, D.C. *Design and Analysis of Experiments*, 9th ed.; Wiley: Hoboken, NJ, USA, 2017.
24. Stat-Ease, Inc. *Design-Expert® Software—Overview/Handbook*. Available online: https://www.statease.com/docs/ (accessed on 24 August 2025).
25. Szpisják-Gulyás, N.; Borbás, R.; Nagy, T. Box–Behnken and Central Composite Designs in Practice: Guidance for Robust Response-Surface Modeling. *Period. Polytech. Chem. Eng.***2023**, *67*, 287–300. (If no DOI is assigned) Available online: https://pp.bme.hu/ch (accessed on 24 August 2025).
26. Chen, M.; Luo, Y.; Xie, Y.; Liu, Y.; Li, Z.; Liu, L. Antiviral Properties of the Natural Product Eugenol: A Review. *Fitoterapia***2025**, *175*, 105731. https://doi.org/10.1016/j.fitote.2025.105731. PubMed
27. Wani, A.R.; Yadav, K.; Khursheed, A.; Rather, M.A. An Updated and Comprehensive Review of the Antiviral Potential of Essential Oils and Their Chemical Constituents with Special Focus on Their Mechanism of Action Against Various Influenza and Coronaviruses. *Microb. Pathog.***2021**, *152*, 104620. PMC
28. Iqhrammullah, M.; Rizki, D.R.; Purnama, A.; Duta, T.F.; Harapan, H.; Idroes, R.; Ginting, B. Antiviral Molecular Targets of Essential Oils against SARS-CoV-2: A Systematic Review. *Sci. Pharm.***2023**, *91*, 15.
29. Ćavar Zeljković, S.; Schadich, E.; Džubák, P.; Hajdúch, M.; Tarkowski, P. Antiviral Activity of Selected Lamiaceae Essential Oils and Their Monoterpenes against SARS-CoV-2. *Front. Pharmacol.***2022**, *13*, 893634.
30. da Silva, J.K.R.; Figueiredo, P.L.B.; Byler, K.G.; Setzer, W.N. Essential Oils as Antiviral Agents. Potential of Essential Oils to Treat SARS-CoV-2 Infection: An In-Silico Investigation. *Int. J. Mol. Sci.***2020**, *21*, 3426.

31. Garozzo, A.; Timpanaro, R.; Stivala, A.; Bisignano, G.; Castro, A.; Stefani, S. Activity of *Melaleuca alternifolia* (Tea Tree) Oil on Influenza Virus A/PR/8: Study on the Mechanism of Action. *Lett. Appl. Microbiol.***2011**, *52*, 781–786. https://doi.org/10.1111/j.1472-765X.2011.03066.x. PubMed
32. Pyankov, O.V.; Usachev, E.V.; Pyankova, O.; Agranovski, I.E. Inactivation of Airborne Influenza Virus by Tea Tree and Eucalyptus Oils. *Aerosol Sci. Technol.***2012**, *46*, 1295–1302. https://doi.org/10.1080/02786826.2012.708949. Taylor & Francis Online
33. Astani, A.; Reichling, J.; Schnitzler, P. Screening for Antiviral Activities of Isolated Compounds from Essential Oils. *Evid.-Based Complement. Altern. Med.***2011**, *2011*, 253643. https://doi.org/10.1093/ecam/nep187. PMC
34. Torres Neto, L.; et al. Essential Oils Block Cellular Entry of SARS-CoV-2 Delta Variant in Human Lung Cells. *Sci. Rep.***2022**, *12*, 21350. https://doi.org/10.1038/s41598-022-25342-8. Nature
35. Rizzuti, B.; Grande, F.; Conforti, F.; Jimenez-Alesanco, A.; Ceballos-Laita, L.; Ortega-Alarcon, D.; Vega, S.; Reyburn, H.T.; Abian, O.; Velazquez-Campoy, A. Sub-Micromolar Inhibition of SARS-CoV-2 3CLpro by Natural Compounds. *Pharmaceuticals***2021**, *14*, 1107. https://doi.org/10.3390/ph14111107. MDPI
36. Jin, Z.; et al. (RCSB PDB Entry 6LU7) Crystal Structure of COVID-19 Main Protease in Complex with an Inhibitor N3, 2020. https://doi.org/10.2210/pdb6lu7/pdb. RCSB PDB
37. Cheung, J.; et al. (wwPDB Entry 3TRK) Structure of the Chikungunya Virus nsP2 Protease, 2011. https://doi.org/10.2210/pdb3trk/pdb. wwpdb.org
38. Norris, M.J.; et al. Structure of the Measles Virus Matrix (M) Protein. *Sci. Adv.***2022**, *8*, eabq3128. (PDB: 7SKS). RCSB PDB
39. Zhang, W.; Chipman, P.R.; Corver, J.; Johnson, P.R.; Zhang, Y.; Mukhopadhyay, S.; Baker, T.S.; Strauss, J.H.; Rossmann, M.G.; Kuhn, R.J. Visualization of Membrane Protein Domains by Cryo-EM: Flavivirus E Conformational Change. *Structure***2004**, *12*, 1607–1618. (PDB: 1TG8). RCSB PDB
40. Sugiyama, K.; Obayashi, E.; Kawaguchi, A.; Suzuki, Y.; Tame, J.R.H.; Nagata, K.; Park, S.Y. Structural Insight into PB1–PB2 Interaction in Influenza Virus Polymerase. *EMBO J.***2009**, *28*, 1803–1811. (PDB: 2ZTT). https://doi.org/10.1038/emboj.2009.138. PMC
41. Bowden, T.A.; Aricescu, A.R.; Gilbert, R.J.; Grimes, J.M.; Jones, E.Y.; Stuart, D.I. Structural Basis of Nipah and Hendra Virus Attachment to Their Cell-Surface Receptor Ephrin-B2. *Nat. Struct. Mol. Biol.***2008**, *15*, 567–572. (PDB: 2VSM). https://doi.org/10.1038/nsmb.1435. EMBL-EBI
42. Białońska, A.; Merten, C.; et al. Structural Basis for Covalent Inhibition of Chikungunya Virus Cysteine Protease nsP2pro. *Proc. Natl. Acad. Sci. USA***2024**, *121*, e2400793121. https://doi.org/10.1073/pnas.2400793121. PNAS
43. Wang, S.; Huang, C.; Wu, W.; Liu, C.; Lin, Y. Chikungunya nsP2: Pleiotropic Functions in Viral Replication and Host Interaction. *Pathogens***2025**, *14*, 83. https://doi.org/10.3390/pathogens14020083. PMC
44. Zhou, T.; et al. Identification of Pockets on the Dengue Virus E Protein and Evaluation of Drugs Targeting Them by Molecular Docking. *Proc. Natl. Acad. Sci. USA***2008**, *105*, 110–115.

https://doi.org/10.1073/pnas.0708964105. PMC

45. Dassanayake, R.S.; et al. Rational Design of Phytochemical Inhibitors Targeting Dengue Virus E Protein: A Computational Approach. *Int. J. Mol. Sci.* **2022**, *23*, 13947. https://doi.org/10.3390/ijms232213947. MDPI
46. Hoque, M.T.; Dey, B.; Hosen, S.Z.; Islam, M.S.; Abdullah-Al-Mamun, M. In Silico Prediction of Potential Inhibitors for Nipah Virus Glycoproteins. *J. Genet. Eng. Biotechnol.* **2023**, *21*, 56. https://doi.org/10.1186/s43141-023-00464-w. ScienceDirect
47. Yoo, C.-B.; Han, K.-T.; Cho, K.-S.; Ha, J.; Park, H.-J.; Nam, J.-H.; Kil, U.-H.; Lee, K.-T. Eugenol isolated from the essential oil of *Eugenia caryophyllata* induces a reactive oxygen species-mediated apoptosis in HL-60 human promyelocytic leukemia cells. *Cancer Lett.* **2005**, *225*, 41–52.
48. Zari, A.T.; Zari, T.A.; Hakeem, K.R. Anticancer properties of eugenol: A review. *Molecules* **2021**, *26*, 7407. https://doi.org/10.3390/molecules26237407. PMC
49. Shapira, S.; Pleban, S.; Kazanov, D.; Tirosh, P.; Arber, N. Terpinen-4-ol: A novel and promising therapeutic agent for human gastrointestinal cancers. *PLoS ONE* **2016**, *11*, e0156540. https://doi.org/10.1371/journal.pone.0156540. PLOS
50. Di Martile, M.; Garzoli, S.; Sabatino, M.; Valentini, E.; D'Aguanno, S.; Ragno, R.; Del Bufalo, D. Antitumor effect of *Melaleuca alternifolia* essential oil and its main component terpinen-4-ol in combination with target therapy in melanoma models. *Cell Death Discov.* **2021**, *7*, 127. https://doi.org/10.1038/s41420-021-00510-3. PubMed
51. Abraham, S.K. Anti-genotoxicity of trans-anethole and eugenol in mice. *Food Chem. Toxicol.* **2001**, *39*, 493–498. https://doi.org/10.1016/S0278-6915(00)00156-3. PubMed
52. Joint FAO/WHO Expert Committee on Food Additives (JECFA). trans-Anethole. *WHO JECFA Database*; WHO Food Additives Series No. 42; World Health Organization: Geneva, Switzerland, 1999. Available online: https://apps.who.int/food-additives-contaminants-jecfa-database/chemical.aspx?chemID=2295 (accessed on 27 August 2025). WHO Apps
53. Selectivity index—an overview. *ScienceDirect Topics*. Available online: https://www.sciencedirect.com/topics/biochemistry-genetics-and-molecular-biology/selectivity-index (accessed on 27 August 2025). ScienceDirect
54. Xiao, X.; Wang, C.; Chang, D.; Wang, Y. Identification of potent and safe antiviral therapeutic candidates against SARS-CoV-2. *Front. Immunol.* **2020**, *11*, 586572. https://doi.org/10.3389/fimmu.2020.586572. FrontiersPMC

Figures

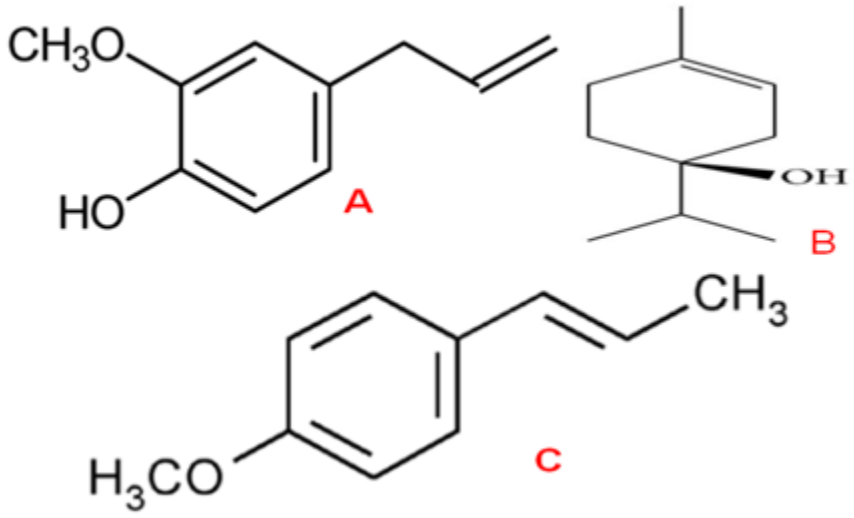


Figure 1

Structure of eugenol[A], Terpinen-4-ol [B] and anethole [C]

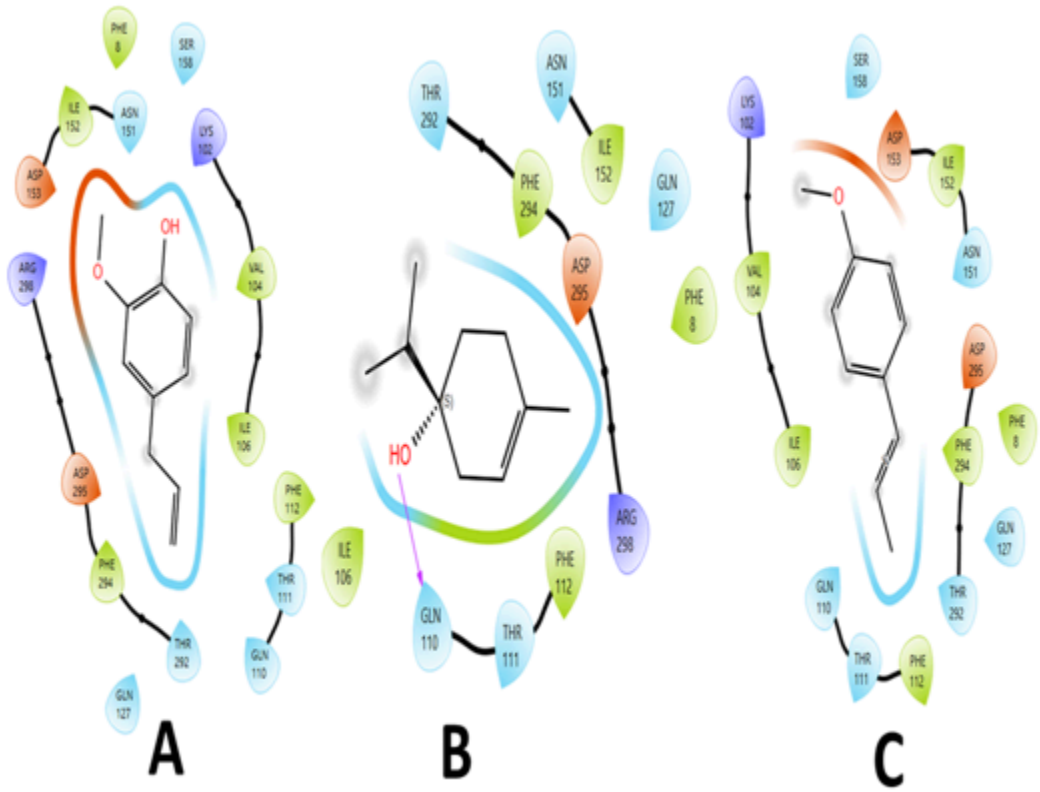


Figure 2

(A–C). Molecular interaction diagrams of SARS-CoV-2 main protease (6LU7) with phytoconstituents. (A) Eugenol predominantly engaged hydrophobic residues such as PHE8, ILE152, and PHE294. (B) Terpinen-4-ol formed an additional hydrogen bond with GLN110, enhancing complex stability. (C) Anethole mainly

relied on hydrophobic contacts, indicating relatively weaker stabilization compared to eugenol and terpinen-4-ol.

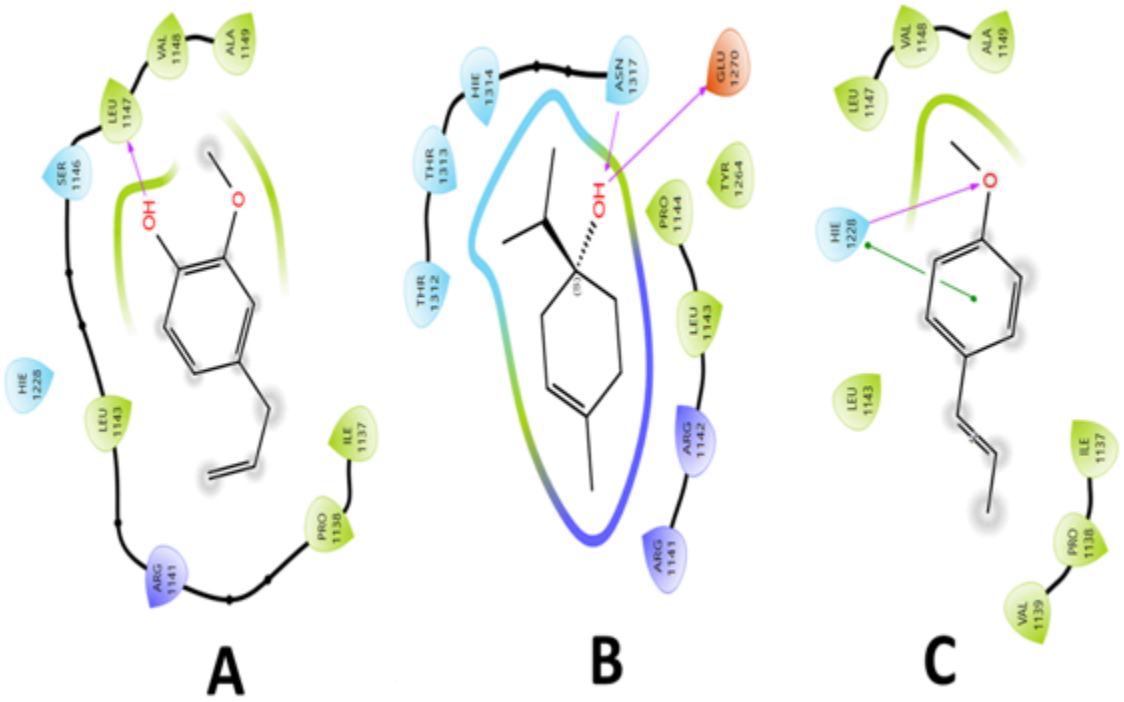


Figure 3

A–C. Molecular interaction diagrams of Chikungunya virus protease (3TRK) with phytoconstituents. (A) Eugenol formed a hydrogen bond with LEU1147, along with hydrophobic contacts stabilizing its binding. (B) Terpinen-4-ol established dual hydrogen bonds with GLU1270 and ASN1317, conferring a stronger and more stable orientation. (C) Anethole engaged in π–π stacking with HIE1228 and multiple hydrophobic interactions, indicating a distinct binding mode compared to eugenol and terpinen-4-ol.

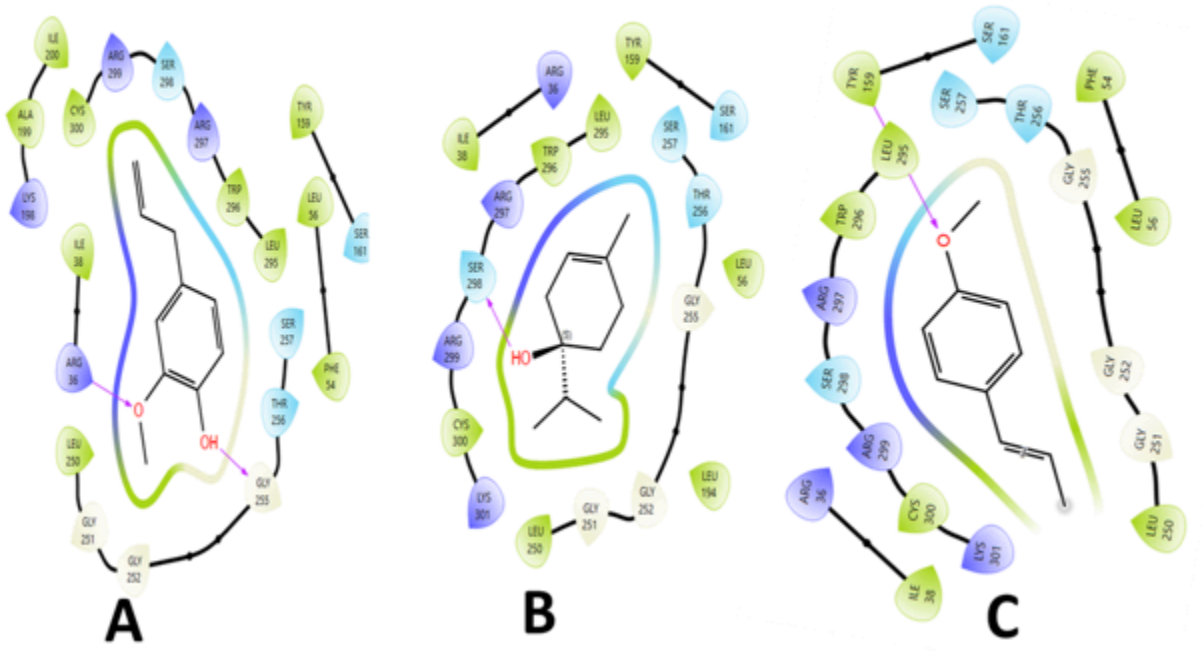


Figure 4

A–C. Molecular interaction diagrams of Measles virus matrix protein (7SKS) with phytoconstituents. (A) Eugenol engaged ARG36 and GLY255 through hydrogen bonding, accompanied by hydrophobic stabilization. (B) Terpinen-4-ol formed a hydrogen bond with SER298, reinforcing its binding orientation. (C) Anethole interacted with TYR159 via hydrogen bonding, along with hydrophobic contacts. Hydrophobic packing around TRP296, LEU295, and CYS300 was a shared stabilizing feature across all ligands.

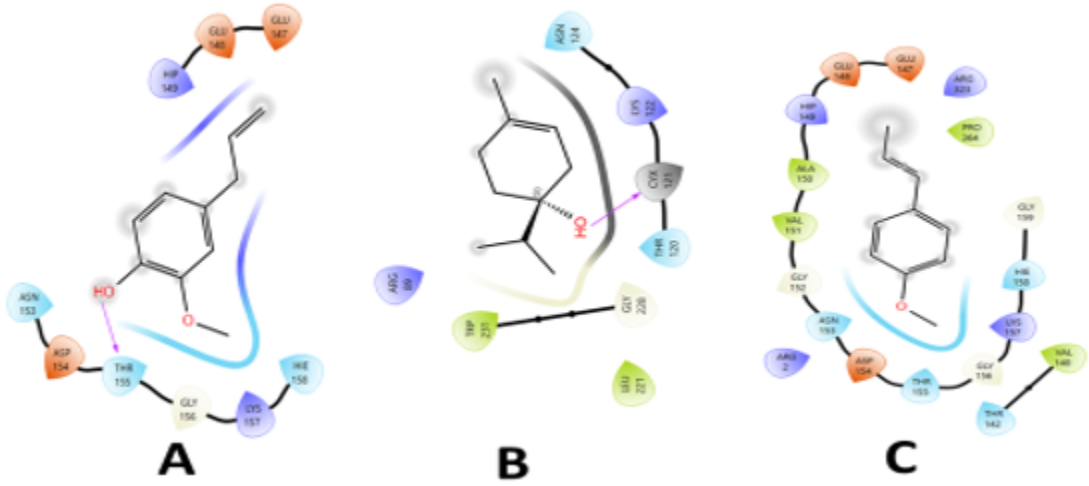


Figure 5

A–C. Molecular interaction diagrams of Dengue virus E glycoprotein (1TG8) with phytoconstituents. (A) Eugenol formed a stabilizing hydrogen bond with THR155. (B) Terpinen-4-ol engaged CYS121 through

hydrogen bonding, enhancing binding affinity. (C) Anethole primarily interacted via hydrophobic residues such as PRO364 and VAL140, indicating a distinct binding mode compared to eugenol and terpinen-4-ol.

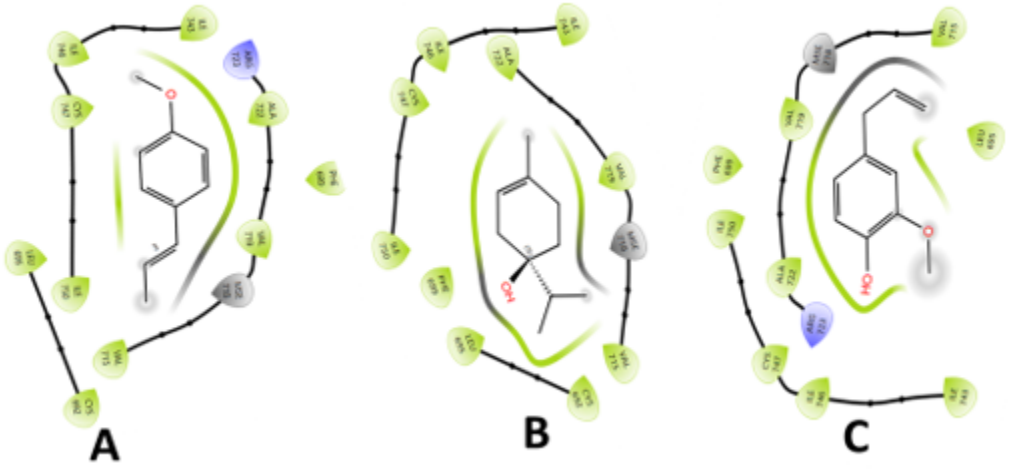


Figure 6

A–C. Molecular interaction diagrams of Influenza PB1–PB2 polymerase (2ZTT) with phytoconstituents. All three ligands bound within a predominantly hydrophobic pocket. (A) Anethole engaged residues such as ARG723, ILE717, and CYS716 through nonpolar interactions. (B) Terpinen-4-ol established hydrophobic contacts with residues including PHE699 and LEU693. (C) Eugenol showed the strongest orientation by forming multiple nonpolar interactions with ILE743, CYS747, and PHE699, suggesting enhanced stabilization.

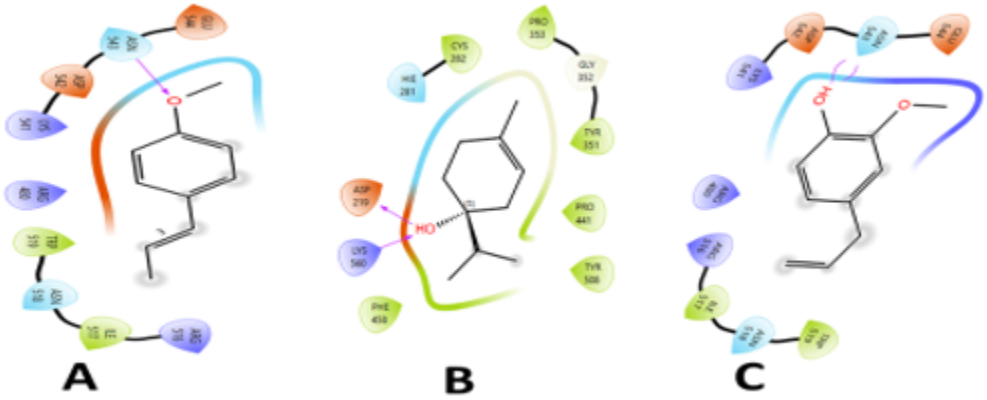


Figure 7

A–C. Molecular interaction diagrams of Nipah virus attachment glycoprotein (2VSM) with phytoconstituents. (A) Eugenol formed a hydrogen bond with ASN543 alongside hydrophobic interactions. (B) Terpinen-4-ol established two stabilizing hydrogen bonds with ASP219 and LYS560, complemented by hydrophobic anchoring. (C) Anethole also engaged ASN543 through hydrogen

bonding but relied more heavily on hydrophobic contacts. Terpinen-4-ol demonstrated comparatively enhanced binding, consistent with its moderately better docking score.

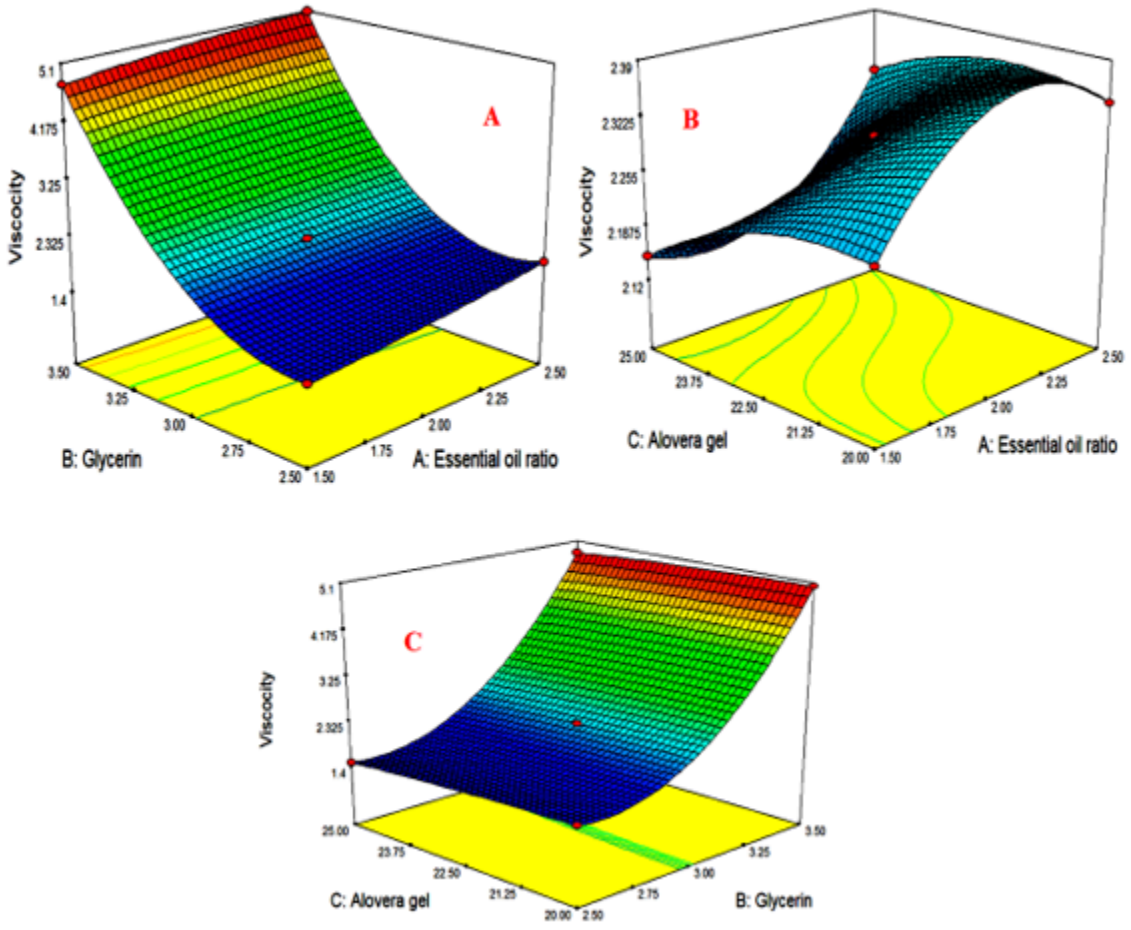


Figure 8

8A-Response surface plots of factor Q_2 vs. Q_1 against Viscosity; 8**B** - Response surface plots of factor Q_3 vs. Q_2 against Viscosity; **8C**- Response surface plots of factor Q_3 vs. Q_1 against Viscosity

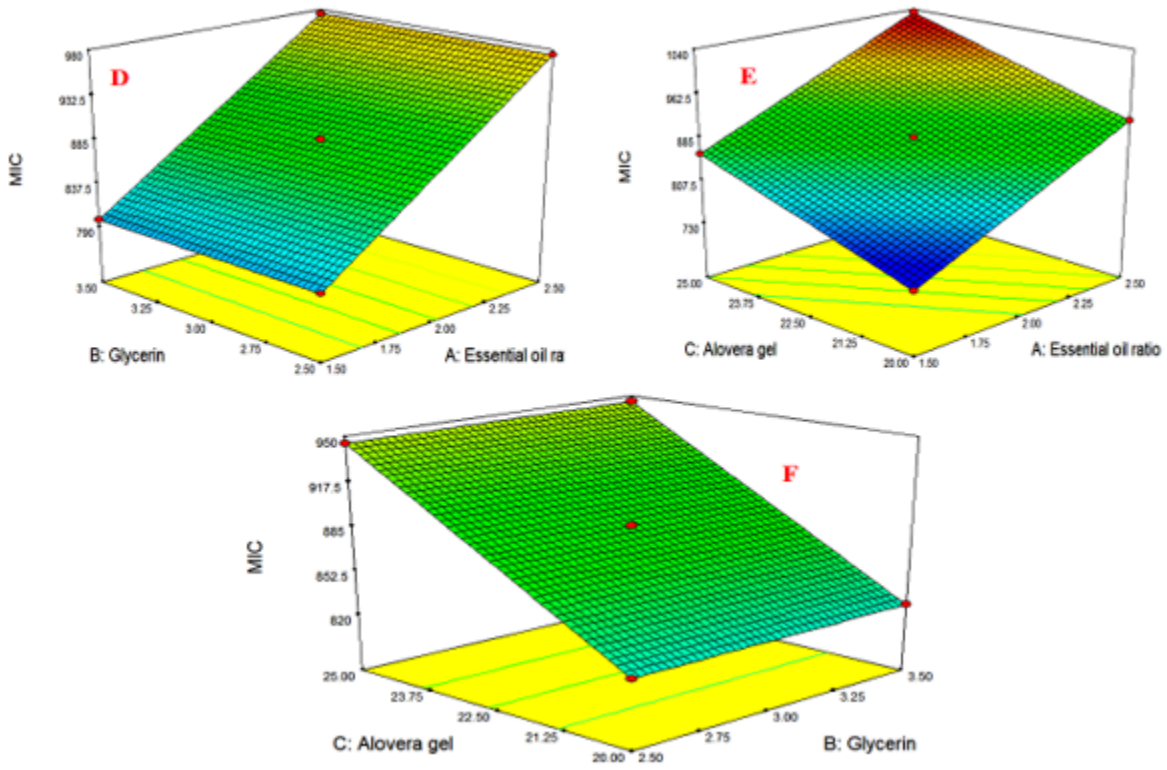


Figure 9

9D-Response surface plots of factor Q_2 vs. Q_1 against MIC; 9**E** - Response surface plots of factor Q_3 vs. Q_2 against MIC; **9F**- Response surface plots of factor Q_3 vs. Q_1 against MIC

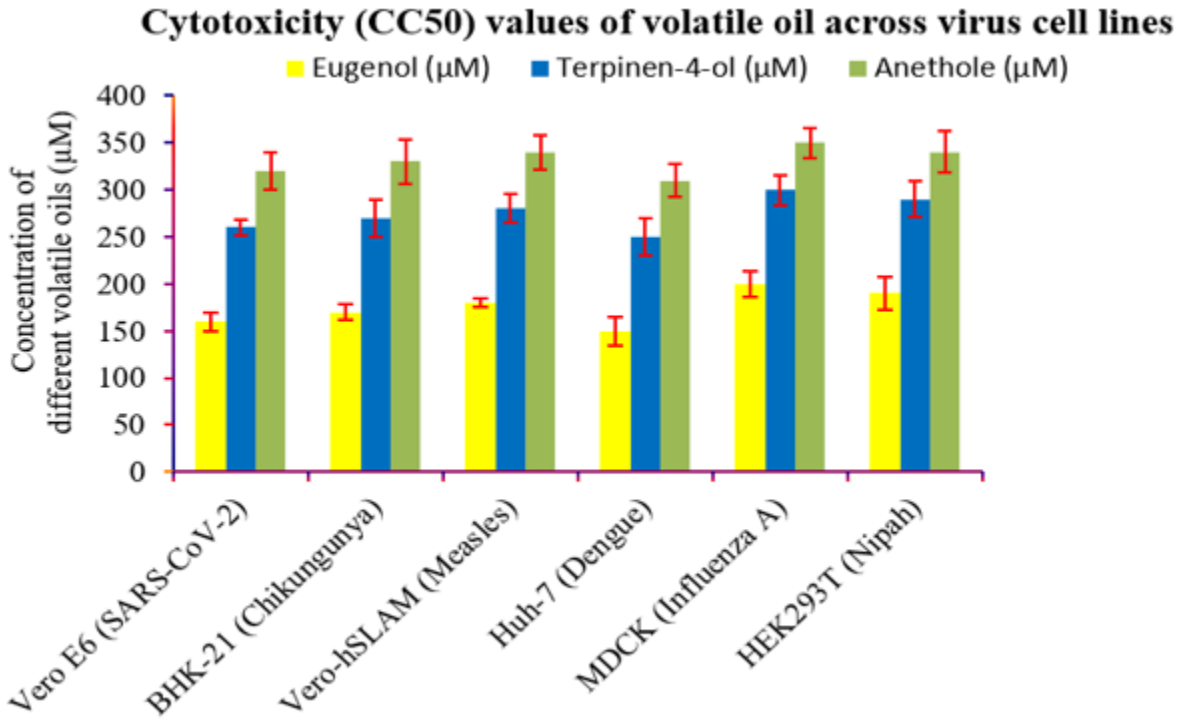


Figure 10

Cytotoxicity (CC_{50}) of volatile-oil constituents across virus-relevant cell lines. Bar plot of Eugenol**,** Terpinen-4-ol, and Anethole (μM) on Vero E6 (SARS-CoV-2), BHK-21 (Chikungunya), Vero-hSLAM (Measles), Huh-7 (Dengue), MDCK (Influenza A), and HEK293T (Nipah). Higher CC_{50} indicates lower cytotoxicity; Anethole shows the highest CC_{50} (least cytotoxic), Terpinen-4-ol is intermediate, and Eugenol the lowest (most cytotoxic) across most lines. Error bars represent variability (SD).